doi:10.1093/jmcb/mjab057
Published online September 16, 2021

Article

Pyk2 suppresses contextual fear memory in an autophosphorylation-independent manner

Jin Zheng[1,2,†], Lun Suo[1,3,†,*], Yuxiao Zhou[1,2,†], Liling Jia[1,2,†], Jingwei Li[1,2], Yanping Kuang[3], Donghong Cui[4], Xuehong Zhang[1], and Qiang Wu[1,2,*]

[1] Center for Comparative Biomedicine, Ministry of Education Key Lab of Systems Biomedicine, State Key Laboratory of Oncogenes and Related Genes, Joint International Research Laboratory of Metabolic and Developmental Sciences, Institute of Systems Biomedicine, School of Life Sciences and Biotechnology, Shanghai Jiao Tong University, Shanghai 200240, China
[2] WLA Laboratories, Shanghai, China
[3] Department of Assisted Reproduction, Shanghai Ninth People's Hospital, Shanghai Jiao Tong University School of Medicine, Shanghai 200011, China
[4] Shanghai Mental Health Center, Shanghai Key Laboratory of Psychotic Disorders, Shanghai Jiao Tong University School of Medicine, Shanghai 200030, China
[†] These authors contributed equally to this work.
[*] Correspondence to: Qiang Wu, E-mail: qiangwu@sjtu.edu.cn; Lun Suo, E-mail: suoyunfei123@gmail.com

Edited by Zhen-Ge Luo

Clustered protocadherins (Pcdhs) are a large family of cadherin-like cell adhesion proteins that are central for neurite self-avoidance and neuronal connectivity in the brain. Their downstream nonreceptor tyrosine kinase Pyk2 (proline-rich tyrosine kinase 2, also known as Ptk2b, Cakb, Raftk, Fak2, and Cadtk) is predominantly expressed in the hippocampus. We constructed *Pyk2*-null mouse lines and found that these mutant mice showed enhancement in contextual fear memory, without significant change in auditory-cued and spatial-referenced learning and memory. In addition, by preparing Y402F mutant mice, we observed that Pyk2 suppressed contextual fear memory in an autophosphorylation-independent manner. Moreover, using high-throughput RNA sequencing, we found that immediate early genes, such as *Npas4*, *cFos*, *Zif268/Egr1*, *Arc*, and *Nr4a1*, were enhanced in *Pyk2*-null mice. We further showed that Pyk2 disruption affected pyramidal neuronal complexity and spine dynamics. Thus, we demonstrated that Pyk2 is a novel fear memory suppressor molecule and *Pyk2*-null mice provide a model for understanding fear-related disorders. These findings have interesting implications regarding dysregulation of the Pcdh–Pyk2 axis in neuropsychiatric disorders.

Keywords: Pyk2 cell adhesion kinase, protocadherin, genetics, spine dynamics, fear memory

Introduction

Fear responses to environmental threats endow human beings to seek comfort and to avoid danger, thus increasing the chances for survival. Dysfunction in fear memory maintenance or retrieval has evolutionary disadvantages, whereas hyperfunction in this capacity leads to mental illnesses, including posttraumatic stress disorder or phobia responses. Thus, it is required for human beings to maintain a dynamic balance between fear memory strengthening and suppression. For memory strengthening, a number of molecules including neurotransmitters (Ben Mamou et al., 2006), transcription factors (Ramamoorthi et al., 2011), and intracellular signaling molecules such as MAPK were found to be important (Paul et al., 2007). In contrast, multiple repressive molecules and signaling pathways are important in fear memory suppression (Cho et al., 2015).

For the assembly of neural circuits in the brain, the clustered protocadherin (Pcdh)–cell adhesion kinase (CAK) signaling pathway might play critical roles in keeping a balance between neurite connection and repulsion (Mountoufaris et al., 2018; Wu and Jia, 2021). In particular, two CAKs, proline-rich tyrosine kinase 2 (Pyk2) and focal adhesion kinase (Fak), function downstream of the clustered Pcdh proteins to regulate cytoskeletal reorganization (Chen et al., 2009; Garrett et al., 2012; Suo et al., 2012; Fan et al., 2018). Pcdhs are a large family of diverse cadherin-like cell adhesion proteins that are encoded by three closely-linked gene clusters, which are arrayed in tandem on a single chromosomal

Received July 16, 2021. Accepted July 19, 2021.

locus and specifically expressed on the cell surface of neurons in the brain (Supplementary Figure S1A; Wu and Maniatis, 1999; Mountoufaris et al., 2018; Wu and Jia, 2021). Individual neurons only express a particular subset of clustered *Pcdh* genes determined by chromatin topological insulators and specific long-distance promoter–enhancer looping interactions within a CTCF/cohesin-mediated SuperTAD (Supplementary Figure S1B; Guo et al., 2015; Jiang et al., 2017; Jia et al., 2020). Homophilic adhesion between extracellular ectodomains of clustered Pcdh proteins is essential for proper assembly of neuronal connectivity (Schreiner and Weiner, 2010; Thu et al., 2014; Brasch et al., 2019). For example, homophilic recognition between the same sets of clustered Pcdh proteins may lead to repulsion, thus self-avoidance and even spacing, between neurites from the same neurons through intracellular signaling and cytoskeletal remodeling (Supplementary Figure S1C; Chen et al., 2009, 2017; Lefebvre et al., 2012; Fan et al., 2018). The mechanisms underlying the adhesive recognition-lead repulsion are not known but may involve signaling molecules such as CAKs (Pyk2 and Fak) and small GTPases.

Pyk2 is a nonreceptor tyrosine kinase and is very abundantly expressed in the hippocampus, reaching maximal levels in adulthood (Avraham et al., 1995; Lev et al., 1995; Sasaki et al., 1995; Yu et al., 1996; Menegon et al., 1999). Pyk2 activity is silenced through autoinhibition of the kinase domain by the N-terminal four band–ezrin–radixin–moesin (FERM) domain, and Pyk2 autoinhibition state could be relieved by autophosphorylation activity mediated by the tyrosine residue at the 402 position (Y402) (Eide et al., 1995; Lev et al., 1995; Dikic et al., 1996; Girault et al., 1999; Park et al., 2004). Autophosphorylation of the Pyk2 Y402 site induces a conformational change and relieves the blocking of the kinase domain by FERM (Lietha et al., 2007; Han et al., 2009; Loving and Underbakke, 2019). Autophosphorylated Pyk2 then recruits c-Src through docking on the phosphorylated Y402 site via the c-Src SH2 domain (Dikic et al., 1996; Lakkakorpi et al., 2003; Park et al., 2004). Finally, the docked c-Src phosphorylates the tyrosine residues at the 576 and 577 positions on the activation loop to fully activate Pyk2 as well as at tyrosine 881 on the C-terminal FAT domain for Pyk2 scaffolding function (Dikic et al., 1996; Lakkakorpi et al., 2003; Park et al., 2004; Fan et al., 2018). Thus, autophosphorylation of tyrosine 402 is the key step in the Pyk2 maximal activation.

Pyk2 plays important roles in neuronal morphogenesis and synaptic plasticity via cytoskeletal dynamics (Huang et al., 2001; Hsin et al., 2010; Suo et al., 2012; Kinoshita et al., 2014; Giralt et al., 2017; Fan et al., 2018; Lee et al., 2019). Pyk2 is postsynaptically located and interacts with NMDA receptors (Heidinger et al., 2002) or PSD95 (Bartos et al., 2010), implicating a role of Pyk2 in both long-term potentiation (Henley and Nishimune, 2001; Huang et al., 2001) and long-term depression (Hsin et al., 2010). Pyk2 has also been identified as a susceptibility locus for late-onset Alzheimer disease and dementia based on genome-wide association studies and implicated in neuronal signaling pathway impairing synaptic functions (Lambert et al., 2013; Beecham et al., 2014; Salazar et al., 2019). Here, we found Pyk2 as a repressor of contextual fear memory based on behavioral studies using gene-modified mice by CRISPR.

Results

Generation of Pyk2 mutant mice

To determine the physiological function of *Pyk2 in vivo*, we generated *Pyk2* mutant mice using CRISPR/Cas9 system. We designed sgRNA-target sequences (gene ID: 19229 from 63961711 to 63961730) based on the first coding exon of the *Pyk2* gene (Figure 1A) and transcribed sgRNA and Cas9 mRNA *in vitro*. After injection into fertilized eggs, two lines of frame-shifted null mutant mice (*Pyk2*-KO$^{-8\ bp}$ and *Pyk2*-KO$^{+1\ bp}$) were generated. Germline transmission of these null alleles was initially screened by *Bsl*I enzyme digestion of the polymerase chain reaction (PCR) products from the tail DNA of pups (Figure 1B–D) and then confirmed by Sanger sequencing.

To validate the knockout phenotype of mutant mice, we detected an immunoreactive band at 116 kDa corresponding to Pyk2 in hippocampal samples from wild-type (WT) but not *Pyk2*-KO mice (Figure 1E). Immunohistochemistry experiments showed that the Pyk2 protein was predominantly expressed throughout the adult hippocampus (Figure 1F) but not in embryonic day 18.5 (E18.5) nor in postnatal day 0 (P0) hippocampus (Supplementary Figure S2). In cornu ammonis 1 (CA1), CA2, CA3, and dentate gyrus (DG) regions of the hippocampus, Pyk2 was mainly found in the cytoplasm and dendrite of pyramidal and granule neurons (Figure 1H–K). In contrast, *Pyk2*-KO mice showed no signal (Figure 1G).

Pyk2 suppresses contextual fear memory in an autophosphorylation-independent manner

Hippocampus is an important organ for learning and memory in the central nervous system. We assessed two hippocampal-dependent learning and memory behavior tests, including associate fear conditioning (Makuch et al., 2011) and Morris water maze (Morris, 1984; Volk et al., 2013) using WT and *Pyk2*-KO mice. For fear conditioning, mice were put into a training chamber for adaptive training on Day 1. Fear training was performed on Day 2 (Figure 2A). On Day 3, mice were put back into the training chamber to test contextual fear conditioning. This was followed by placing the animals into a novel chamber to test novel contextual fear conditioning or into a novel chamber and exposed to the original auditory cues to test trace fear conditioning. After repeated fear training using auditory cues on Day 2, we found increases in frequencies of fear responses but no difference between the WT and *Pyk2*-KO$^{-8\ bp}$ mice (Figure 2B), indicating that memory acquisition and fear responses were intact in the *Pyk2*-KO$^{-8\ bp}$ mice. On Day 3, fear response of the *Pyk2*-KO$^{-8\ bp}$ homo mice were significantly increased compared with their WT littermates when the mice were put back into the training context 24 h after training

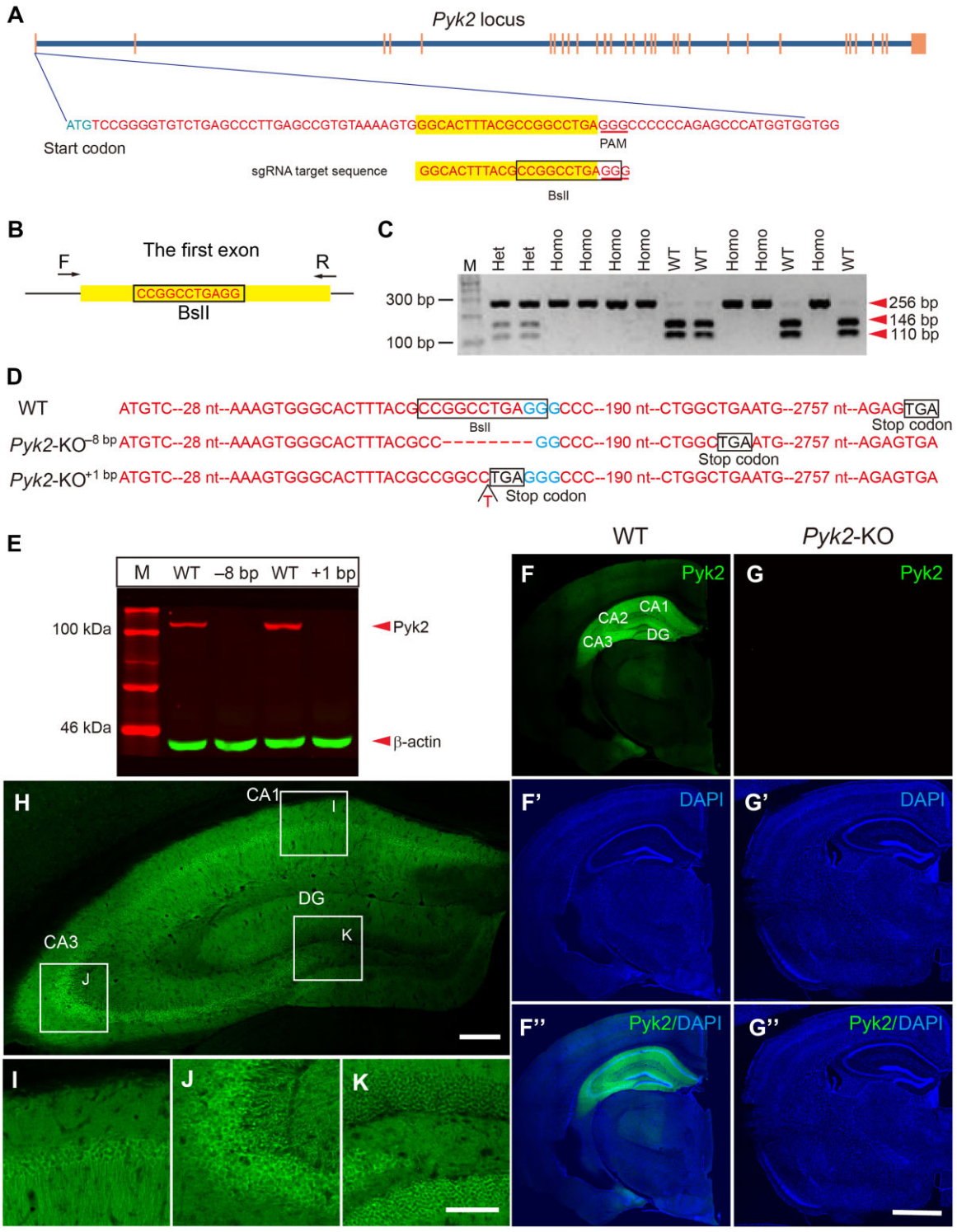

Figure 1 Prominent and specific expression patterns of *Pyk2* in the mouse hippocampus. (**A**) Schematic of the Cas9/sgRNA-targeting sequence of the *Pyk2* gene by CRISPR. The sgRNA-targeting sequence is highlighted in yellow and the protospacer adjacent motif (PAM) is underlined. (**B**) The forward (F) and reverse (R) primers for PCR and the *Bsl*I restriction enzyme site at the target regions are indicated. (**C** and **D**) Electrophoresis of genotyping PCR products from mouse tails after restriction enzyme digestion (**C**) and its confirmation by Sanger sequencing (**D**). (**E**) Validation of the absence of Pyk2 proteins in the mouse hippocampus by gene disruption in both *Pyk2*-KO$^{-8\ bp}$ and *Pyk2*-KO$^{+1\ bp}$ by western blotting. (**F** and **G**) Confocal images of brain sections from WT and *Pyk2*-KO mice immunostained with a specific antibody against Pyk2 (**F**, **G**), DAPI (**F′**, **G′**), or merged (**F″**, **G″**). Scale bar, 1000 μm. (**H**–**K**) Enlarged pictures of the hippocampus were indicated for pyramidal and granule cells. Scale bar, 200 μm (**H**) and 100 μm (**I**–**K**).

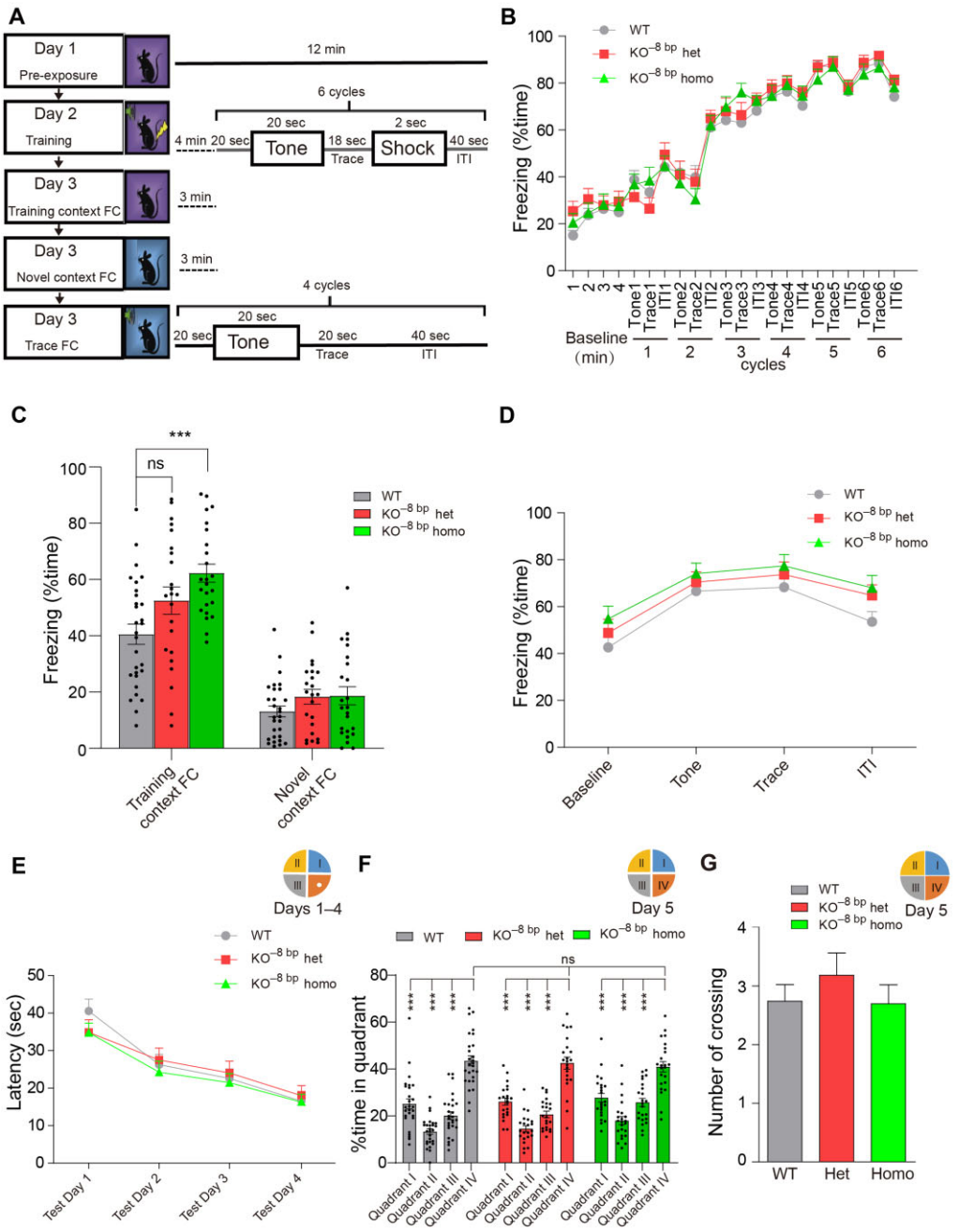

Figure 2 Hippocampal-dependent contextual fear memory is enhanced in *Pyk2*-KO$^{-8\ bp}$ mice. (**A**) The procedure for fear conditioning tests. (**B**) Trace fear responses in the *Pyk2*-KO$^{-8\ bp}$ homo ($n = 24$), *Pyk2*-KO$^{-8\ bp}$ het ($n = 23$), and WT ($n = 29$) mice were significantly enhanced during training but without significant differences among genotypes [$F_{times}(21, 1533) = 152.69$, $P < 0.0001$; $F_{genotype}(2, 1533) = 0.31$, $P = 0.74$]. The two-way repeated-measure ANOVA test. (**C**) *Pyk2*-KO$^{-8\ bp}$ homo mice exhibited significantly higher fear response than that of WT mice (*Pyk2*-KO$^{-8\ bp}$ homo = 62.26%, *Pyk2*-KO$^{-8\ bp}$ het = 52.50%, WT = 40.54%, homo vs. WT, $P < 0.001$; het vs. WT, $P > 0.05$) in the training context at 24 h posttraining. In a novel context, fear responses showed no difference between genotypes (*Pyk2*-KO$^{-8\ bp}$ homo-= 18.68%, *Pyk2*-KO$^{-8\ bp}$ het = 18.35%, WT = 13.15%, homo vs. WT, $P > 0.05$; het vs. WT, $P > 0.05$). The one-way ANOVA, Bonferroni *post hoc* test. (**D**) Auditory trace fear conditioning was unaffected in the *Pyk2*-KO$^{-8\ bp}$ homo and *Pyk2*-KO$^{-8\ bp}$ het mice 24 h after training [$F_{sessions}(3, 219) = 30.31$, $P < 0.0001$; $F_{genotype}(2, 219) = 2.20$, $P > 0.05$; *Pyk2*-KO$^{-8\ bp}$ homo, $n = 24$; *Pyk2*-KO$^{-8\ bp}$ het, $n = 23$; WT, $n = 29$]. The two-way ANOVA test. (**E**) During the initial acquisition of a hidden platform location, escape latencies in Morris water maze tests were similar among genotypes of *Pyk2*-KO$^{-8\ bp}$ homo ($n = 23$), *Pyk2*-KO$^{-8\ bp}$ het ($n = 22$), and WT ($n = 27$) mice [$F_{times}(3, 207) = 38.36$, $P < 0.0001$; $F_{genotype}(2, 207) = 0.46$, $P > 0.05$]. The two-way ANOVA test. (**F**) *Pyk2*-KO$^{-8\ bp}$ homo, *Pyk2*-KO$^{-8\ bp}$ het, and WT mice showed a significant preference for the target quadrant (quadrant IV) at test Day 5 [$F_{quadrants}(3, 207) = 104.13$, $P < 0.0001$]. The two-way ANOVA, Bonferroni *post hoc* test. However, there was no significant difference among genotypes [$F_{genotype}(2, 207) = 3.08$, $P > 0.05$]. (**G**) There was also no significant difference among genotypes in the number of times that the position of the escape platform was crossed [$F_{genotype}(2, 69) = 0.65$, $P > 0.05$]. Data are represented as mean ± SEM.

(Figure 2C). In contrast, both *Pyk2*-KO$^{-8\ bp}$ and WT mice showed no significant phenotypic difference in freezing behavior when the animals were put into a novel context only (Figure 2C) or novel context together with the auditory tone (Figure 2D). Finally, we observed similar contextual fear memory phenotype for the *Pyk2*-KO$^{+1\ bp}$ mice (Supplementary Figure S3A–C). Collectively, these data indicated that *Pyk2*-KO mice are more capable of contextual-associative fear memory maintenance than the auditory-cued memory maintenance.

We also performed Morris water maze tests, consisting of 2 days of training, 4 days of acquisition, followed by the probe test (Supplementary Figure S3D). During initial spatial memory learning, we found that *Pyk2*-KO$^{-8\ bp}$ and WT mice exhibited similar escape latency durations during testing from Day 1 to Day 4 when the platform was put in quadrant IV (Figure 2E), indicating that the mice acquired spatial memory equally well between genotypes. When the hidden platform was removed from the pool on Day 5 of testing, both WT and *Pyk2*-KO$^{-8\ bp}$ mice showed a persistence of entries to the quadrant of the old platform (Figure 2F) and no significant difference was found between genotypes in crossing times of the platform location (Figure 2G). Finally, we observed similar Morris-test behaviors for the *Pyk2*-KO$^{+1\ bp}$ mice (Supplementary Figure S3E–G). These data indicated similar spatial memory formation between WT and *Pyk2*-KO mice.

Because autophosphorylation at tyrosine 402 is a crucial step in Pyk2 activation, we generated Pyk2-autophos phorylation-site mutant mice with the tyrosine residue 402 changed into phenylalanine (Pyk2^{Y402F}) (Supplementary Figure S4A–C). This autophosphorylation-site mutant mice were then tested for contextual-associated memory, auditory-cued memory, and Morris water maze. Of interest, the Pyk2^{Y402F} mice showed no difference in either fear memory acquisition (Supplementary Figure S4D) or contextual fear memory (Supplementary Figure S4E) and auditory-cued fear memory (Supplementary Figure S4F), as well as spatial-cued memory (Supplementary Figure S4G–I). Finally, we confirmed the autophosphorylation defects of Pyk2^{Y402F} proteins in the hippocampus by western blotting (Supplementary Figure S5). In conjunction with aberrant contextual fear memory enhancements of *Pyk2*-KO mice (Figure 2; Supplementary Figure S3), these data demonstrated that Pyk2 suppresses contextual fear memory in an autophosphorylation-independent manner.

Pyk2 re-expression rescues contextual fear memory behavioral phenotype

To test the specificity of CRISPR/Cas9 knockout and to rule out potential off-target effects, we performed the rescue experiments. We used adeno-associated viral (AAV) system to re-express either Pyk2 (AAV-Pyk2-3×FLAG) or a control GFP protein (AAV-control) (Figure 3A) by injecting the virus stereotaxically into the dorsal and ventral hippocampus (Figure 3B). Three weeks after the virus injection, Pyk2 or GFP was expressed in the hippocampus (Figure 3C and D). Quantification showed that re-expressed Pyk2 levels were ∼86% of the WT Pyk2 levels (Figure 3E). Hippocampal re-expression of Pyk2 rescues the contextual associative fear phenotype of Pyk2 knockout (Figure 3F and G), with no obvious effect on the auditory-cued fear memory (Figure 3H). These results demonstrated definitively that the enhanced contextual fear memory behavior is due to Pyk2 knockout but not off-target effect.

Pyk2 represses immediate early genes (IEGs) after fear conditioning

To test potential roles of Pyk2 in hippocampal gene regulation, we compared the transcriptome profiles of the hippocampi between WT and *Pyk2*-KO mice after fear conditioning using high-throughput RNA sequencing (RNA-seq). According to cutoff thresholds of >2-fold changes or <0.5-fold changes and false discovery rate (FDR) <0.001, a total of 52 RNA transcripts were identified: 17 downregulated and 35 upregulated in *Pyk2*-KO mice compared with that of WT mice (Figure 4A–C; Supplementary Table S1). Among the upregulated genes, we found neuronal activity-regulated genes and early-response genes, including *Npas4*, c*Fos*, *Zif268/Egr1*, *Arc*, and *Nr4a1* (Figure 4C), which were illustrated in a representative UCSC browser image (Figure 4D) and were validated by real-time RT-PCR (Supplementary Figure S6). Remarkably, upregulation of these early-response genes only was detected after fear conditioning in the *Pyk2*-KO mice but not under basal conditions or in the Pyk2-rescued mice (Supplementary Figure S6). As previous studies reported, for normal fear conditioning training, IEG expression in mice increased from 10 to 30 min and then followed by a significant decrease at 4 h after training (Figure 4E; Cho et al., 2015). These normal gene expression dynamics might be beneficent to keep a balance between memory consolidation and suppression. Interestingly, our work found that the expression levels of these genes after behavioral tests were significantly increased when *Pyk2* was deleted (Figure 4E), indicating that *Pyk2* signaling might act as a key control in regulating IEG expression. However, as expected, none of the neuronal activity genes mentioned above was found to be differentially expressed in the hippocampus between Pyk2^{Y402F} mutant and the WT littermate mice (Supplementary Table S2). This could explain why the Pyk2^{Y402F} mutant mice showed no enhancement in contextual-dependent fear memory maintenance. Finally, two members of the clustered Pcdhs, *Pcdhα5 and Pcdhαc1*, were upregulated in the *Pyk2*-KO mice (Figure 4C; Supplementary Table S1) and two distinct members, *Pcdhα3 and Pcdhα7*, were dysregulated in the Pyk2^{Y402F} mice (Supplementary Table S2). This suggests that there might be feedback regulation of clustered *Pcdh* gene expression by Pyk2 in both autophosphorylation-dependent and independent manners.

Morphological changes of hippocampal neurons in the Pyk2-KO mice

To test whether disruption of Pyk2 affected neuronal morphology and synaptic plasticity, we performed Golgi staining of the pyramidal neurons from WT and *Pyk2*-KO littermate mice. As shown in Figure 5A–D, hippocampal neurons in CA1, CA2, CA3, and DG

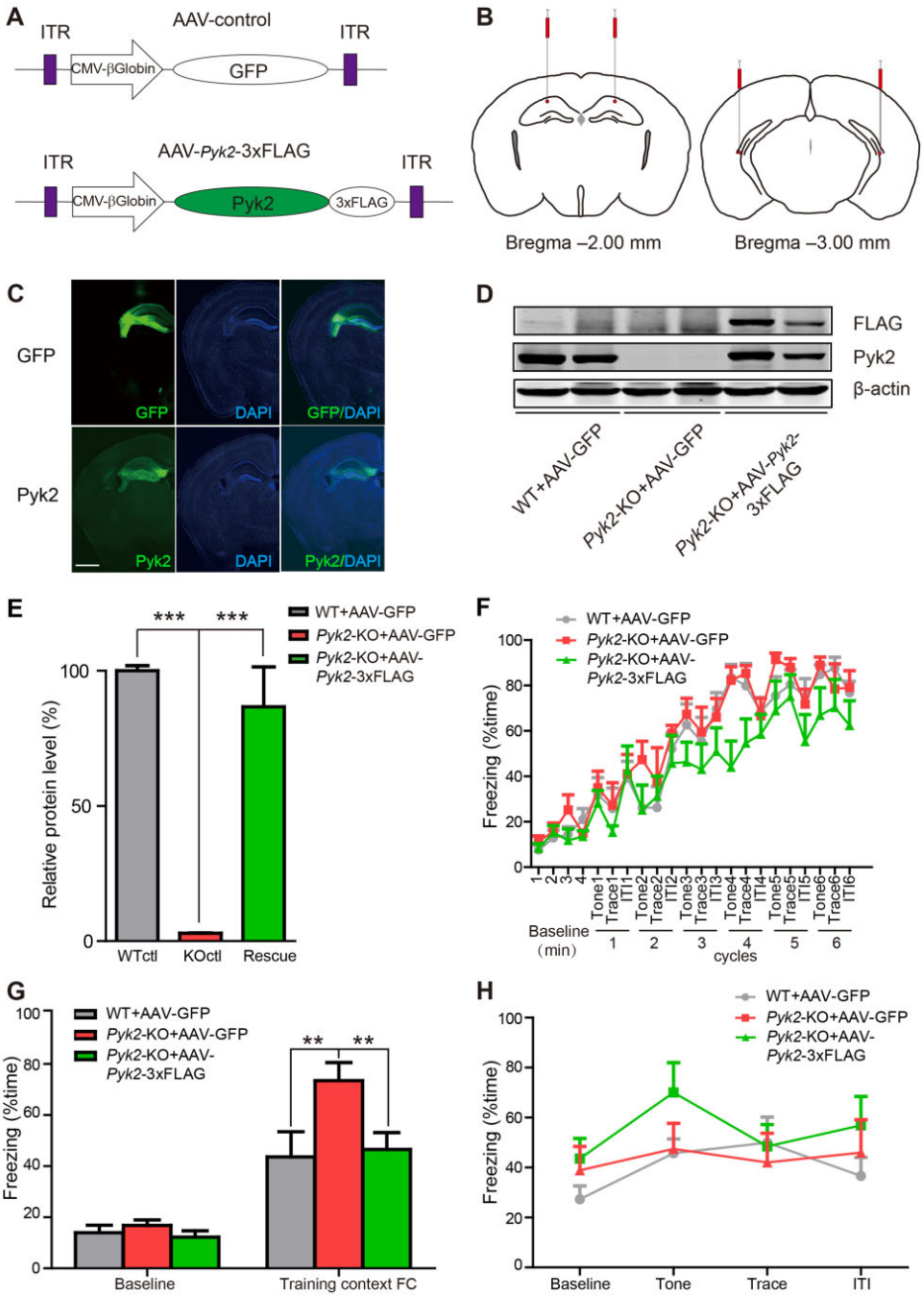

Figure 3 Pyk2 re-expression in the hippocampus rescues the contextual fear memory behavioral phenotype. (**A**) AAV constructs used to express GFP (control) or Pyk2 proteins, ITR, inverted terminal repeats. (**B**) Illustration of bilateral viral injections into the mouse dorsal and ventral hippocampus. (**C**) Typical images for expression of GFP or re-expression of Pyk2-3×FLAG proteins in the *Pyk2*-KO mouse hippocampus. Scale bar, 1000 μm. (**D**) Western blotting for validation of successful expression of GFP or Pyk2 proteins in the hippocampus from three groups: WT + AAV-GFP ($n = 6$), *Pyk2*-KO + AAV-GFP ($n = 4$), and *Pyk2*-KO + AAV-Pyk2-3×FLAG ($n = 4$). (**E**) Quantification of western blotting in **D**. WT + GFP = 100%, *Pyk2*-KO + GFP = 2.92%, *Pyk2*-KO + Pyk2-3×FLAG = 86.57%, $P < 0.0001$. The one-way ANOVA, Bonferroni *post hoc* test. (**F**–**H**) Performance during the fear conditioning training process (**F**), contextual fear memory test 24 h after training (**G**), and auditory-cued fear memory test (**H**) of the WT mice injected with AAV-GFP ($n = 7$) and the *Pyk2*-KO mice injected with AAV-GFP ($n = 6$) or AAV-Pyk2-3×FLAG ($n = 6$). (**F**) All genotypes showed enhanced fear response during training [$F_{time}(21, 336) = 42.18$, $P < 0.0001$], without significant differences between genotypes [$F_{genotype}(2, 336) = 2.05$, $P = 0.16$]. (**G**) During baseline, all genotypes of mice showed similar fear responses. By contrast, the *Pyk2*-KO + AAV-GFP mice showed enhanced contextual fear memory than the WT + AAV-GFP mice (WT + AAV-GFP = 43.64%, *Pyk2*-KO + AAV-GFP = 73.48%, $P < 0.01$), and re-expression of Pyk2 proteins in the hippocampus of *Pyk2*-KO mice (*Pyk2*-KO + AAV-Pyk2-3×FLAG = 46.53%) rescued contextual fear memory behavioral phenotype ($P < 0.01$). (**H**) No difference was observed between genotypes during the cue-induced fear memory test [$F_{genotype}(2, 48) = 0.88$, $P = 0.44$]. The two-way ANOVA, Bonferroni *post hoc* test.

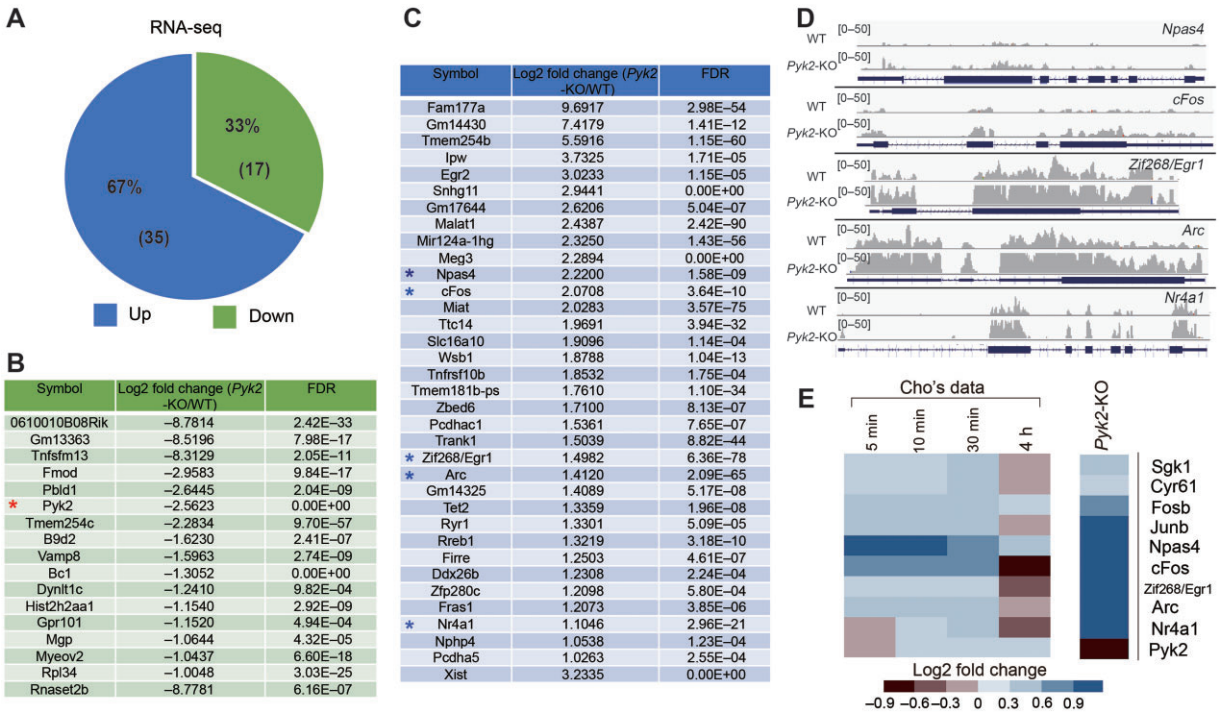

B

Symbol	Log2 fold change (*Pyk2*-KO/WT)	FDR
0610010B08Rik	–8.7814	2.42E–33
Gm13363	–8.5196	7.98E–17
Tnfsfm13	–8.3129	2.05E–11
Fmod	–2.9583	9.84E–17
Pbld1	–2.6445	2.04E–09
* Pyk2	–2.5623	0.00E+00
Tmem254c	–2.2834	9.70E–57
B9d2	–1.6230	2.41E–07
Vamp8	–1.5963	2.74E–09
Bc1	–1.3052	0.00E+00
Dynlt1c	–1.2410	9.82E–04
Hist2h2aa1	–1.1540	2.92E–09
Gpr101	–1.1520	4.94E–04
Mgp	–1.0644	4.32E–05
Myeov2	–1.0437	6.60E–18
Rpl34	–1.0048	3.03E–25
Rnaset2b	–8.7781	6.16E–07

C

Symbol	Log2 fold change (*Pyk2*-KO/WT)	FDR
Fam177a	9.6917	2.98E–54
Gm14430	7.4179	1.41E–12
Tmem254b	5.5916	1.15E–60
Ipw	3.7325	1.71E–05
Egr2	3.0233	1.15E–05
Snhg11	2.9441	0.00E+00
Gm17644	2.6206	5.04E–07
Malat1	2.4387	2.42E–90
Mir124a-1hg	2.3250	1.43E–56
Meg3	2.2894	0.00E+00
* Npas4	2.2200	1.58E–09
* cFos	2.0708	3.64E–10
Miat	2.0283	3.57E–75
Ttc14	1.9691	3.94E–32
Slc16a10	1.9096	1.14E–04
Wsb1	1.8788	1.04E–13
Tnfrsf10b	1.8532	1.75E–04
Tmem181b-ps	1.7610	1.10E–34
Zbed6	1.7100	8.13E–07
Pcdhac1	1.5361	7.65E–07
Trank1	1.5039	8.82E–44
* Zif268/Egr1	1.4982	6.36E–78
* Arc	1.4120	2.09E–65
Gm14325	1.4089	5.17E–08
Tet2	1.3359	1.96E–08
Ryr1	1.3301	5.09E–05
Rreb1	1.3219	3.18E–10
Firre	1.2503	4.61E–07
Ddx26b	1.2308	2.24E–04
Zfp280c	1.2098	5.80E–04
Fras1	1.2073	3.85E–06
* Nr4a1	1.1046	2.96E–21
Nphp4	1.0538	1.23E–04
Pcdha5	1.0263	2.55E–04
Xist	3.2335	0.00E+00

Figure 4 Loss of *Pyk2* activates the expression of multiple neuronal activity-related genes in the hippocampus. (**A**) Pie chart showing genes up- and downregulated in the hippocampus of *Pyk2*-KO mice. (**B** and **C**) Seventeen downregulated (**B**) and 35 upregulated (**C**) differentially epressed genes in *Pyk2*-KO mice were ranked by fold changes. *Pyk2* is marked with a red asterisk and IEGs are marked with blue asterisks. (**D**) UCSC genome browser images showing transcription increases in *Pyk2*-KO mice by RNA-seq of selected neuronal activity-related genes. (**E**) Expression patterns of some IEGs in fear condition training under normal conditions [left panel from sequencing data by Cho et al. (2015)] or in *Pyk2*-KO mice (right panel from our sequencing data).

regions of the *Pyk2*-KO$^{-8\ bp}$ mice showed higher morphological complexity in dendrites than that of WT mice. Quantification of the reconstructed confocal images revealed significant increases in total length (Figure 5E), the number of branch points (bifurcations) (Figure 5F), and segments between branch points (Figure 5G) in the *Pyk2*-KO$^{-8\ bp}$ mice. Furthermore, the proportion of spines with a classical head shape was significantly increased, whereas that of spines with branched heads was significantly decreased in *Pyk2* mutants (Figure 5H–J). Similar results were observed for the *Pyk2*-KO$^{+1\ bp}$ mice (Supplementary Figure S7). Remarkably, the hippocampal neurons from the Pyk2^{Y402F} mice did not show higher dendrite complexity than that of WT mice (Supplementary Figure S8).

To further confirm the role of *Pyk2* in dendritic development, we transfected GFP-encoding plasmids into primary-cultured hippocampal neurons for better tracing of dendrite morphology (Figure 5K and L). As shown in Figure 5M, the spine density of dendritic segments was significantly increased in *Pyk2*-KO neurons compared with WT control neurons. However, there were significant decreases in the spine length (Figure 5N) and spine width (Figure 5O) in *Pyk2*-KO neurons. Interestingly, time-lapse tests also indicated that the spine remodeling was more stable with less structural plasticity when *Pyk2* was deleted (Figure 5P and Q; Supplementary Movies S1 and S2), which could explain why *Pyk2* disruption induces contextual fear memory maintenance, as stable spine has been known as a potential structural basis for long-term memory storage (Grutzendler et al., 2002). Taken together, these data suggested a role of the Pyk2 proteins in dendrite formation and spine dynamics, which was critical for fear memory.

Discussion

The cellular and molecular mechanisms of fear memory acquisition and maintenance have been extensively studied in the amygdala (Herry and Johansen, 2014; Janak and Tye, 2015), whereas some other brain structures, including superior colliculus (Shang et al., 2015), thalamus (Do-Monte et al., 2015), and cortex (Cembrowski and Spruston, 2016; Xu et al., 2016), as well as hippocampus (Wu et al., 2017) also contribute to this biological process. Here, through analyzing gene expression, dendrite morphology, and synaptic structural plasticity, in conjunction with mouse genetics, we found that Pyk2 functions as a contextual fear memory suppressor protein capable of regulating neuronal activity in an autophosphorylation-independent manner. The fear suppressor role of Pyk2 is consistent with its stress-modulating function (Sheehan et al., 2003; Kinoshita et al., 2014; Montalban et al., 2019).

Our *Pyk2*-KO mice grew up to the adult stage with normal body weights and showed predicted ratios of genotypes in line with Mendelian inheritance, similar to the *Pyk2*-KO mice

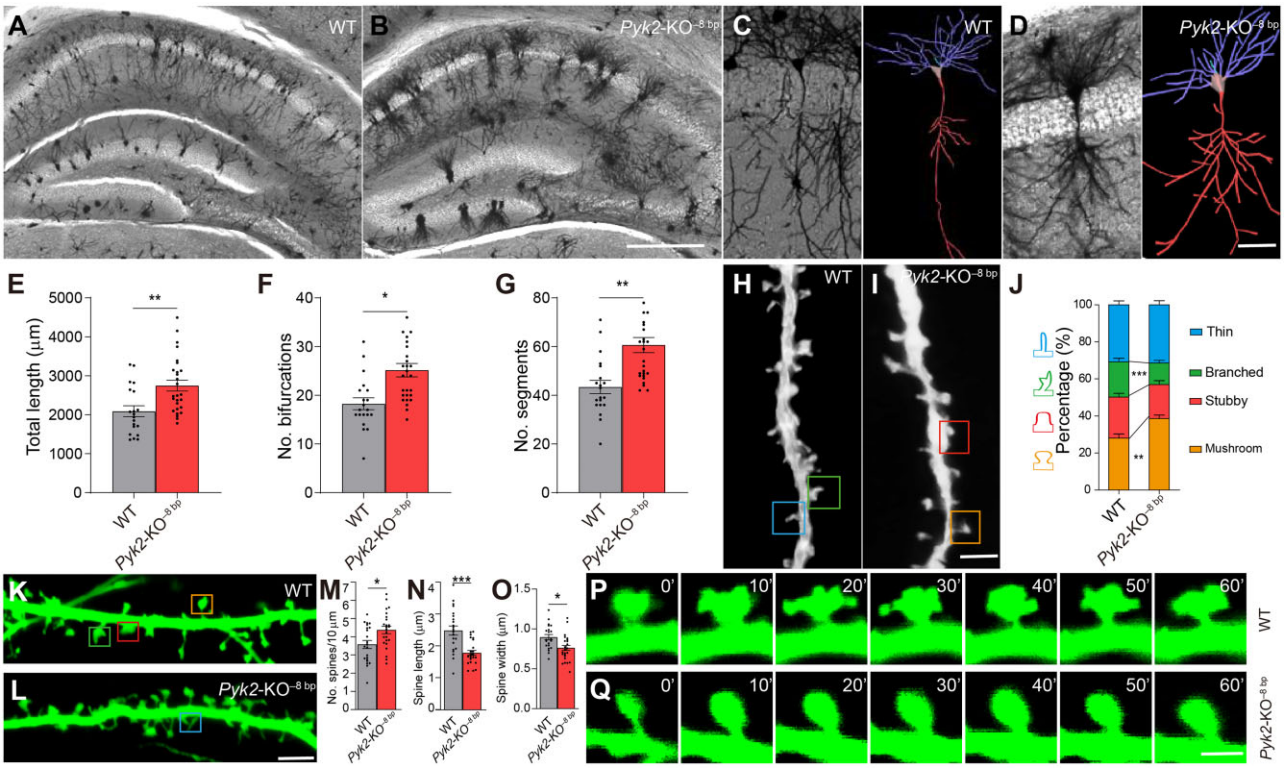

Figure 5 Morphology of hippocampal neurons in *Pyk2*-KO mice. (**A**–**D**) Representative Golgi staining sections and reconstructed 3D confocal images of the CA1 hippocampal neurons from the WT (**A**, **C**) and *Pyk2*-KO$^{-8\ bp}$ (**B**, **D**) littermates. Scale bar, 400 μm (**A** and **B**) and 50 μm (**C** and **D**). (**E**–**G**) Quantification of total length (**E**), branch points (bifurcation) (**F**), and the number of segments (**G**) between branch points (WT, $n = 20$; *Pyk2*-KO$^{-8\ bp}$, $n = 27$; $^{*}P < 0.05$, $^{**}P < 0.01$). (**H** and **I**) Representative confocal images of the basal dendritic segments from the CA1 pyramidal neurons of the WT (**H**) and *Pyk2*-KO$^{-8\ bp}$ (**I**) mice. Scale bar, 3 μm. (**J**) Spine morphology analyses (WT, $n = 584$ spines of 35 dendritic segments; *Pyk2*-KO$^{-8\ bp}$, $n = 754$ spines of 43 dendritic segments) of basal dendritic neurons ($^{**}P < 0.01$, $^{***}P < 0.001$). (**K** and **L**) Representative images of spines in dendritic segments of 14 DIV neurons from the WT (**K**) or *Pyk2*-KO$^{-8\ bp}$ (**L**) mice. Scale bar, 5 μm. (**M**–**O**) Quantification of the spine density (**M**), length (**N**), and width (**O**) (WT, $n = 370$ spines of 22 dendritic segments; *Pyk2*-KO$^{-8\ bp}$, $n = 452$ spines of 24 dendritic segments). (**P** and **Q**) Representative confocal images of spine structural dynamics of hippocampal neurons from the WT (**P**) and *Pyk2*-KO$^{-8\ bp}$ (**Q**) mice in time-lapse experiments at every 10-min interval for a total of 1 h. Scale bar, 2 μm. Data are represented as mean ± SEM.

previously generated (Okigaki et al., 2003; Giralt et al., 2017). *Pyk2* is predominantly expressed throughout CA1, CA2, CA3, and DG regions of the hippocampus in the adult mice (Figure 1) and rats (Menegon et al., 1999) but not at the embryonic 18.5 and P0 stages (Supplementary Figure S2), indicating that *Pyk2* is dispensable for embryonic neurogenesis, neuronal differentiation, and brain development. Based on the hippocampal-specific expression pattern, we speculate that Pyk2 might be a critical molecular component involved in cognitive behaviors and associated with psychiatric disorders relevant to dysfunction in learning and memory processes.

Two classic hippocampal-dependent learning and memory tests, Pavlovian fear conditioning and Morris water maze, demonstrated that the acquisition of contextual fear and spatial-referenced memories is not affected in *Pyk2*-KO mice. By contrast, contextual fear memory maintenance was enhanced when *Pyk2*-KO mice were put back into the training context 24 h after training, indicating that molecular mechanisms and neuronal circuitries responsible for contextual-cued fear memory are increased in the *Pyk2*-KO mice, consistent with a suppressor role of Pyk2 in memory maintenance.

It is interesting that Pyk2 specifically suppressed contextual fear memory but had no effect on spatial memory although both of them depend on the hippocampus. Consistent with our results, a recent study with a separate *Pyk2*-KO line found no alteration of spatial memory (Salazar et al., 2019). However, another study found that Pyk2 in dorsal hippocampus had a role in spatial memory (Giralt et al., 2017). We conducted fear conditioning tests with our two *Pyk2*-KO mouse lines and found that Pyk2 suppressed contextual fear memory but not auditory-cued memory, which is more sensitive to amygdala lesion (Phillips and LeDoux, 1992). This suggests a suppressor role of Pyk2 in the hippocampus but not amygdala in regulating contextual fear memory, which is consistent with predominant Pyk2 expression in the hippocampus but not amygdala (Figure 2). Finally, re-expression of Pyk2 in the hippocampus is

enough to rescue the aberrant enhancement of contextual fear memory (Figure 3). All in all, these data suggested complex roles of Pyk2 in different types of memories.

Pyk2, a close homologue of Fak, is a nonreceptor tyrosine kinase capable of regulating signaling pathways by relieving its catalytic activity through autophosphorylation (Lev et al., 1995; Lietha et al., 2007). However, we did not find any difference in contextual fear conditioning between $Pyk2^{Y402F}$ autophosphorylation-site mutant and WT control mice (Supplementary Figures S4 and S5), suggesting that Pyk2 functions in fear memory suppression in an autophosphorylation-independent manner.

Pyk2 has a known scaffolding function independent of its kinase activity through recruiting of the Grb2/SOS complex by the phosphorylated residue Y881 (Lev et al., 1995; Dikic et al., 1996; Fan et al., 2018). Specifically, tyrosine 881 could couple Pyk2 to the Grb2/SOS complex and activate specific mitogen-activated protein kinase (MAPK)/extracellular signal-regulated kinase (ERK) signaling pathway, which has been reported to play critical regulatory roles in long-term potentiation-dependent gene expression (Dikic et al., 1996; Davis et al., 2000). Thus, Pyk2 might suppress contextual fear memory through regulating Grb2/SOS–MAPK/ERK–CREB signaling pathway (Davis et al., 2000).

Through RNA-seq, we found that a number of CREB-regulated IEGs, encoding neuronal activity-related transcription factors NPAS4, cFOS, Zif268/EGR1, NR4A1, as well as activity-regulated cytoskeletal associated protein (ARC), were significantly increased in the *Pyk2*-KO mice at transcriptional level. Remarkably, expression levels of none of these IEGs were found to be significantly increased in the $Pyk2^{Y402F}$ mice, consistent with no behavioral phenotype. The IEGs have been widely implicated in hippocampal-dependent learning and memory and are believed to play an integral role in synapse-specific plasticity (Shepherd and Bear, 2011). Our study indicated that neurons from the *Pyk2*-KO mice showed more complexity during dendrite arborization. In addition, the proportion of neuronal spines with classic mushroom heads, markers of matured spines, was increased. Finally, the proportion of branched spines was significantly decreased in the *Pyk2*-KO mice. Interestingly, a recent study found decreased spine neck length as well as spine density without alteration of spine head size in homozygous and heterozygous Pyk2-deficient mice (Giralt et al., 2017). Taken together, we suggest that Pyk2 plays an important role in regulating cytoskeletal remodeling and spine dynamics. This is consistent with recent findings that Pyk2 modulates stress-induced responses and drug-induced behavior effects (Montalban et al., 2019; de Pins et al., 2020).

The clustered Pcdh proteins are essential for self-avoidance and tiling of neuronal processes as well as proper assembly of neuronal connectivity and cortical neuron migration (Fukuda et al., 2008; Garrett et al., 2012; Lefebvre et al., 2012; Suo et al., 2012; Chen et al., 2017; Fan et al., 2018). Their mutations or dysregulations are associated with numerous neuropsychiatric and neurodevelopmental disorders (Flaherty and Maniatis, 2020; Jia and Wu, 2020). These Pcdhs negatively regulate CAKs Pyk2 and Fak through the cytoplasmic domains (Chen et al., 2009; Garrett et al., 2012; Suo et al., 2012; Fan et al., 2018). The present study found a novel fear memory suppressive function of Pyk2 through the autophosphorylation-independent scaffolding pathway to IEGs. Interestingly, Pyk2 suppresses contextual fear memory but not the learning process. Recent studies revealed distinct hippocampal pathways for contextual fear learning and memory (Tonegawa et al., 2015; Roy et al., 2017). Future studies will be focused on the identification of hippocampal memory engram cells for this Pyk2-related contextual fear circuitry.

Materials and methods

Establishment of Pyk2 gene-modified mice

Animals were maintained at 23°C in a 12-h (7:00–19:00) light and 12-h (19:00–7:00) dark schedule. All animal experiments were approved by the Institutional Animal Care and Use Committee (IACUC) of Shanghai Jiao Tong University (protocol#: 1602029). Mouse lines deficient for Pyk2 protein were generated using the CRISPR/Cas9 system (Guo et al., 2015; Li et al., 2015; Fan et al., 2018). Briefly, we first selected a sgRNA-target sequence from the first coding exon of the *Pyk2* gene, and then a T7 promoter containing-sgRNA PCR product was amplified from pLKO.1-sgRNA plasmid using oligos, TAATA CGACT CACTA TAGGG GGCAC TTTAC GCCGG CCTGA and GTTTT AGAGC TAGAA ATAG, as forward and reverse primers, respectively. The resultant product was gel-purified and used as a template for *in-vitro* transcription using the MEGA short script T7 kit (Life Technology, AM1354). Cas9 mRNA was transcribed *in vitro* from linearized pcDNA3.1-Cas9 plasmid using the mMACHINE T7 ULTRA kit (Life Technology, AM1345). Both Cas9 mRNA and sgRNAs were purified using the MEGA clear kit (Life Technology, AM1908) and mixed in the RNase-free TE buffer at the concentration of 100 ng/μl. The mixture was injected into the fertilized eggs of the C57BL/6 mice. After equilibration for 30 min, 15–25 injected embryos were transferred into the fallopian tube of pseudopregnant ICR females for generating chimeric mice. Germline transmission and genotyping were confirmed by PCR using allele-specific primers (forward: TTGTC TCTGC AGGAC TGCAA TGTGC; reverse: TACCT GGATC TCTGT CTGCA CTGTG) under the following conditions: 94°C for 2 min; 94°C for 30 sec, 59°C for 30 sec, 72°C for 30 sec, 35 cycles; 72°C for 3 min; held at 4°C. The PCR products were then gel-purified and digested with the *Bsl*I enzyme. Digested DNA was separated on an ethidium bromide-stained agarose gel. For identification of mutations, purified PCR products were used for TA cloning and subsequently for Sanger sequencing.

The method for establishing $Pyk2^{Y402F}$ mutant mice was similar to that of *Pyk2*-KO mice with sgRNA-targeting sequences designed at the 13th exon of the *Pyk2* locus. Furthermore, single-stranded

oligonucleotides (Supplementary Figure S4) were used as a donor DNA with a mutation at Y402 residue and a nonsense mutation at the PAM sequence for coinjection into the fertilized eggs together with Cas9 mRNA and sgRNA. The germline-transmitted mutants were identified by PCR using allele-specific primer pairs (forward: ACTGT GTGGC TTCCT TGAAT CCTGG; reverse: TCTCC TGTGG TGTCC CATGA ATAC) under the following conditions: 94°C for 2 min; 94°C for 30 sec, 59°C for 30 sec, 72°C for 30 sec, 35 cycles; 72°C for 3 min; held at 4°C. PCR products were then purified and confirmed by Sanger sequencing.

Behavioral tests

We used both male and female adult mice at ~3- to 5-month old for behavioral tests. All behavioral experiments were performed blind to genotypes of mice, and independent experimenters were carried out to analyze the data. For contextual and auditory fear conditioning, tests were performed according to previous methods (Makuch et al., 2011; Wahlsten, 2011; Volk et al., 2013) and the protocol was illustrated in Figure 2A. Briefly, mice were put into the training chamber (Clever Sys., Inc.) for 12 min of adaptive training on Day 1. Fear training was performed on Day 2 as the following: mice were allowed to acclimate to the chamber for 4 min prior to 6 cycles of consecutive training, each consisting of a 20-sec baseline, an auditory tone, 18-sec trace interval, 2-sec foot shock, and a 40-sec intertrial interval. On Day 3, mice were put back to the original training chamber for 3 min to assess contextual fear conditioning, after which they were returned to their home cage for 3 min. For trace fear conditioning testing, mice were then placed in a novel chamber different from the training chamber for 3 min as an index of novel contextual fear responses. This was followed by an auditory trace response testing. Percentage of time spent in freezing was recorded using an automated Video FreezeScan system (Clever Sys., Inc.).

For Morris water maze tests, experiments were performed using the previous protocols with minor modifications (Vorhees and Williams, 2006; Wahlsten, 2011; Volk et al., 2013). Briefly, mice were tested in a pool of 120 cm in diameter surrounded by different visual cues. A 10-cm-diameter circular platform was used as the goal platform. Water temperature was maintained at 22°C–23°C. Testing includes three stages of training, acquisition, and probe test. Mice were handled 5 min for consecutive 3 days by experimenters for adaptive training followed by 2 days of training, in which testing was conducted four trials each day and the platform was put visibly at different quadrants for each trial. In the acquisition sessions, the platform was not visible and placed in a fixed location for 4 days. Mice were tested in four trials per day, with a 10-min interval between each trial. A probe test was conducted 24 h after the last acquisition trial. For each trial, mice were placed into the pool at start positions distributed in different quadrants, and the latency to the platform and the number of crossing the putative platform location were automatically recorded using the Clever system software (TopScan3.0).

RNA sequencing and data analyses

Hippocampi collected from 2- to 3-month-old WT and gene-modified mice at 24 h after initial fear conditioning were used for total RNA extraction using TRIzol reagent according to the manufacturer's protocol (Life Technology, 15596018). The concentration of the RNA was measured by NanoDrop 2000. At least 200 ng of total RNA was used for preparing RNA libraries before deep sequencing according to the manufacturer's instructions (Illumina). The cDNA libraries were sequenced on an Illumina HiSeq 2000 instrument with 50-base single-end reads. Raw sequencing data were cleaned and mapped to the mouse reference genome (mm9) using Bowtie2. Relative abundance of transcripts was measured by fragments per kilobase of exon per million mapped fragments (FPKM). Differentially expressed mRNAs between gene-modified and WT mice were identified using the Cuffdiff module, and genes with $>$2-fold or $<$0.5-fold changes and FDR $<$ 0.001 were selected. The data have been deposited into the NCBI Gene Expression Omnibus (GEO) database with the accession number GSE158606 and GSE180598.

Quantification PCR

RNA was purified from dissected hippocampal tissues before and 24 h after fear conditioning. Then, 1000 ng of RNA was reverse-transcribed to cDNA using the HiScript II Q RT SuperMix and quantification PCR was performed using the FastStart SYBR Green Master on an ABI StepOnePlus PCR machine. The genes of interest were normalized to *Gapdh* and shown as fold change over control using the ΔΔCT method. At least three independent replicate mice were used. The primers used for quantification PCR were as follows: *Gapdh*, forward: GGTGA AGGTC GGTGT GAACG, reverse: CTCGC TCCTG GAAGA TGGTG; *Npas4*, forward: CTGCA TCTAC ACTCG CAAGG, reverse: GCCAC AATGT CTTCA AGCTC T; *Egr1*, forward: AGCGA ACAAC CCTAT GAGCA, reverse: TCGTT TGGCT GGGAT AACTC; *Nr4a1*, forward: AAAAT CCCTG GCTTC ATTGA G, reverse: TTTAG ATCGG TATGC CAGGC G; *cFos*, forward: TTTCA ACGCC GACTA CGAGG, reverse: GCGCA AAAGT CCTGT GTGTT; *Arc*, forward: AGTCT TGGGC AGCAT AGCTC, reverse: TTCAC TGGTA TGAAT CACTG GG.

Golgi staining and 3D reconstruction of CA1 pyramidal neurons

Golgi staining experiments were performed as previously described (Suo et al., 2012). Briefly, 4-week-old male *Pyk2*-modified and WT littermates were anesthetized and sacrificed. Brains were collected as quickly as possible and put into the impregnation solution for 14 days. The impregnation solution was then replaced by the solution C for another 3 days. The impregnated brains were then cut into 150-μm sections using a Vibratome (Leica VT1200S). After dehydration, sections were cleared in xylene before mounting using Permount (Fisher Chemical™, SP15-500). Images were collected with a Nikon confocal microscopy (Nikon A1) under a 20× objective for dendritic analyses using the Neuromantic software (http://www.reading.ac.uk/neuromantic/body_index.php). Each CA1

pyramidal neuron was 3D-reconstructed by tracing the dendritic paths of the Z-stacking pictures. The numbers of branch points (bifurcations) and segments between branch points were analyzed automatically by the software. For spine analyses, high-resolution images were collected under a 60× oil objective with a 3× digital zooming factor and 0.2 μm Z interval. The Z-stacking images were projected at minimal intensity by Nikon NIS-Elements AR. The reconstructed Z-stacking pictures were imported into the Image J (NIH) and inverted for analyzing the spine morphology. The spine head and neck diameters and the spine length of ∼20 consecutive spines were measured on a single basal dendrite. The spines were categorized based on standard criteria (Zagrebelsky et al., 2005; Cao et al., 2020) as following: (i) mushroom: spine head diameter ≥1.5× neck diameter; (ii) stubby: spine head diameter <1.5× neck diameter and spine length <2× head diameter; (iii) thin: spine head diameter <1.5× neck diameter and spine length ≥2× head diameter; (iv) branched: spines with >1 head. The experimenter and analyzer were blind to genotypes during data analyses.

Immunohistochemistry

Brains removed from embryonic 18.5, P0, and adult mice were fixed in 4% paraformaldehyde (PFA) overnight at 4°C before cutting into 50-μm sections with a Vibratome (Leica VT1200 S). After permeabilized with 0.3% Triton X-100 and blocked with 3% bovine serum albumin (BSA), sections were incubated with a rabbit anti-Pyk2 antibody (Abcam, ab32571) at 4°C overnight. Signals were detected with Alexa 488 Fluor-conjugated secondary antibodies (Invitrogen, A32790). Cell nuclei were visualized with 4′-6-diamidino-2-phenylindole (DAPI).

Hippocampal neuron culture and time-lapse analyses

The hippocampus was collected from E18.5 embryos in Hanks' balanced salt solution with 0.5% glucose, 10 mM HEPES, and 50 μg/ml penicillin/streptomycin. Tissues were digested with 0.25% trypsin for 15 min at 37°C. After stopping the reaction with trypsin inhibitor (0.5 mg/ml) for 3 min at room temperature, tissues were gently triturated in the plating medium (MEM medium, 10% fetal bovine serum, 1 mM glutamine, 10 mM HEPES, and 25 μg/ml penicillin/streptomycin). Cell viability and density were determined using 0.4% trypan blue and a hemocytometer. Cells were plated at the density of 500 cells/mm^2 onto glass coverslips with a uniform application of poly-D-lysine (Thermo, A3890401) and laminin (Thermo, 23017015). Cells were incubated with 5% CO_2 at 37°C. After 3–4 h, the plating medium was replaced with a serum-free culture medium (Neurobasal medium, 2% B27, 0.5 mM glutamine, and 25 μg/ml penicillin/streptomycin supplemented with 25 mM glutamate acid), and thereafter half of the medium (w/o glutamate) was replaced every 3 days. On Day 3, 2 mM cytosine arabinoside (Sigma) was added to inhibit the proliferation of glia. Neurons were transfected with pCAG-EGFP plasmids at 12 days *in vitro* (DIV) using Lipofectamine 2000 (Invitrogen, 11668019) and cultured until 14 DIV before fixing for analyses. For immunofluorescent staining, cultured primary hippocampal neurons were washed with 1× phosphate-buffered saline, fixed in 4% PFA for 20 min at room temperature, washed again, and permeabilized with 0.3% Triton X-100 for 20 min. After blocking with 3% BSA, cells were incubated with rabbit anti-GFP antibody (Invitrogen, A-31852) at 4°C overnight. Signals were detected with Alexa 488 Fluor-conjugated secondary antibodies (Invitrogen, A32790). Cell nuclei were visualized with DAPI. For spine analyses, high-resolution images were collected under a 60× oil objective with a 3× digital zooming factor. For time-lapse analyses, transfected neuronal cells were maintained under physiological conditions with a stage-top microscope incubator, and Z-stack images were acquired on an inverted laser-scanning confocal microscope. Pictures were captured every 1 min for up to 1 h with a 60×, 1.4 numerical aperture objective.

Viral injection

Mice at 3–4 months old were anesthetized with sodium pentobarbital and placed on a stereotaxic apparatus. Small bilateral holes were drilled into the skull, and high titers of AAVs (packaged by Shanghai Taitool Bioscience Co., Ltd), engineered to overexpress GFP or Pyk2-3×Flag were stereotaxically injected into the hippocampus at four sites at the following coordinates relative to bregma (mm): AP −2.0, ML ±2.0, DV −2.0 and AP −3.0, ML ±3.0, DV −3.5 for dorsal and ventral hippocampus, respectively. Then, 0.5 μl AAV-GFP or AAV-Pyk2-3×FLAG (1×10^{13} virus genome/ml) was injected into each site of the hippocampus through a 30-guage Hamilton microsyringe at a rate of 0.1 μl per min using the Quintessential Stereotaxic Injector. After injection, the microsyringe was left in place for an additional 5 min to ensure full virus diffusion. The scalps were sealed and mice were monitored as they recovered from anesthesia. Behavioral experiments were performed 3 weeks after virus injection.

Protein extraction for western blotting

Hippocampi from adult mice were homogenized with RIPA lysis buffer (50 mM Tris–HCl, pH 7.5, 150 mM NaCl, 1% NP40, 0.25% sodium deoxycholate, 10 mM NaF, 10 mM Na_3VO_4, 1 mM phenylmethanesulfonyl fluoride, and protease inhibitors) at 20 μl/mg ratio. The homogenate was centrifuged at 12000 *g* for 20 min and the resulting supernatant was collected and measured with the BCA method. The rabbit anti-Pyk2 antibody (Abcam, ab32571), rabbit anti-phospho-Pyk2 (Tyr402) antibody (Cell Signaling Technology), mouse anti-β-actin antibody (Proteintech Group, 66009-1-Ig), IRDye680-conjugated goat anti-rabbit secondary antibody (Biosciences, 926-68070), and IRDye800-conjugated goat anti-mouse secondary antibody (Biosciences, 926-32213) were used for western blotting. Signals were scanned on the Odyssey system (Li-Cor).

Statistical analyses

Interquartile range (IQR) of data is defined as the distance between the upper and lower quartiles. Data points that are 1.5 IQR more than the upper quartile or less than the lower quartile are outliers, and thereby excluded from analysis of variance (ANOVA).

The response (freezing in the fear condition experiment or latency in the water maze experiment) y_i of measurement i is modeled in two-way ANOVA with repeated measurements

$$y_i = \mu + g_j + m_{k(j)} + t_l + \epsilon_i \,(1),$$

where μ is the basic response, g_j is the fixed factor of genotype j, $m_{k(j)}$ is the random factor of mouse k nested in genotype j, t_l is the fixed factor of treatment l (stimulus in the fear conditioning experiments or quadrant in the water maze experiments), and ϵ_i is the independently identically distributed error of measurement i. ANOVA assumes that ϵ_i satisfies normal distribution with zero mean and unknown uniform variance. The restrictions of Equation (1) are

$$\sum_j g_j = 0,\ \sum_{k(j)} m_{k(j)} = 0,\ \sum_l t_l = 0.$$

To test whether a genotype has a significant influence on the response, ANOVA compares the square error of the full model Equation (1) with that of the reduced model

$$y_i = \mu + m_{k(j)} + t_l + \epsilon_i.$$

Similarly, to test whether stimulus has a significant influence, it compares the full square error with that of

$$y_i = \mu + g_j + m_{k(j)} + \epsilon_i.$$

The one-way ANOVA is just a special case of the two-way ANOVA when there is only one treatment.

Then, we introduce the interaction factor $n_{j,l}$ between genotype and stimulus in the full model Equation (1)

$$y_i = \mu + g_j + m_{k(j)} + t_l + n_{j,l} + \epsilon_i \,(2),$$

where

$$\sum_j n_{j,l} = 0,\ \sum_l n_{j,l} = 0.$$

Adding the restriction $n_{j_1,l} = n_{j_2,l}$ in Equation (2), we obtain a reduced model, which can be used to compare responses between genotypes j_1 and j_2 under stimulus l. To compare stimuli l_1 and l_2 under genotype j, restrict $n_{j,l_1} = n_{j,l_2}$. Pairwise multiple comparisons are corrected by the Bonferroni *post hoc* test.

Data for quantification PCR and dendritic morphology analyses between WT and Pyk2 mutant mice were analyzed using a two-tailed, unpaired Student's *t*-test. Data were represented as mean ± SEM. $^*P < 0.05$, $^{**}P < 0.01$, $^{***}P < 0.001$.

Supplementary material

Supplementary material is available at *Journal of Molecular Cell Biology* online.

Acknowledgments

We thank Prof. Weidong Li (Shanghai Jiao Tong University) for allowing us to use his fear-conditioning testing equipment, Dr Wenjie Bian (Institute of Neuroscience, Chinese Academy of Sciences) for advice on the Golgi staining, and Prof. Aaron Hsueh (Stanford University) for linguistic help.

Funding

This work was supported by grants from the National Natural Science Foundation of China (31200825 to L.S. and 31630039 to Q.W.), the Ministry of Science and Technology of China (2017YFA0504203 and 2018YFC1004504), the Science and Technology Commission of Shanghai Municipality (19JC1412500 and 21DZ2210200 to Q.W.), and Shanghai Jiao Tong University Scientific and Technological Innovation Funds (17JCYB12 to L.S.). Q.W. is a Shanghai Subject Chief Scientist.

Conflict of interest: none declared.

Author contributions: J.Z., L.S., Y.Z., and Q.W. designed experiments; J.Z., L.S., Y.Z., L.J., and J.L. performed experiments; Y.K., D.C., X.Z., and Q.W. supervised experiments; J.Z., L.S., and Q.W. prepared the manuscript.

References

Avraham, S., London, R., Fu, Y., et al. (1995). Identification and characterization of a novel related adhesion focal tyrosine kinase (RAFTK) from megakaryocytes and brain. J. Biol. Chem. *270*, 27742–27751.

Bartos, J.A., Ulrich, J.D., Li, H., et al. (2010). Postsynaptic clustering and activation of Pyk2 by PSD-95. J. Neurosci. *30*, 449–463.

Beecham, G.W., Hamilton, K., Naj, A.C., et al. (2014). Genome-wide association meta-analysis of neuropathologic features of Alzheimer's disease and related dementias. PLoS Genet. *10*, e1004606.

Ben Mamou, C., Gamache, K., and Nader, K. (2006). NMDA receptors are critical for unleashing consolidated auditory fear memories. Nat. Neurosci. *9*, 1237–1239.

Brasch, J., Goodman, K.M., Noble, A.J., et al. (2019). Visualization of clustered protocadherin neuronal self-recognition complexes. Nature *569*, 280–283.

Cao, H., Li, M.Y., Li, G., et al. (2020). Retinoid X receptor α regulates DHA-dependent spinogenesis and functional synapse formation in vivo. Cell Rep. *31*, 107649.

Cembrowski, M.S., and Spruston, N. (2016). Illuminating the neuronal architecture underlying context in fear memory. Cell *167*, 888–889.

Chen, J., Lu, Y., Meng, S., et al. (2009). α- and γ-Protocadherins negatively regulate PYK2. J. Biol. Chem. *284*, 2880–2890.

Chen, W.V., Nwakeze, C.L., Denny, C.A., et al. (2017). Pcdhαc2 is required for axonal tiling and assembly of serotonergic circuitries in mice. Science *356*, 406–411.

Cho, J., Yu, N.K., Choi, J.H., et al. (2015). Multiple repressive mechanisms in the hippocampus during memory formation. Science *350*, 82–87.

Davis, S., Vanhoutte, P., Pages, C., et al. (2000). The MAPK/ERK cascade targets both Elk-1 and cAMP response element-binding protein to control long-term potentiation-dependent gene expression in the dentate gyrus in vivo. J. Neurosci. *20*, 4563–4572.

de Pins, B., Montalban, E., Vanhoutte, P., et al. (2020). The non-receptor tyrosine kinase Pyk2 modulates acute locomotor effects of cocaine in D1 receptor-expressing neurons of the nucleus accumbens. Sci. Rep. *10*, 6619.

Dikic, I., Tokiwa, G., Lev, S., et al. (1996). A role for Pyk2 and Src in linking G-protein-coupled receptors with MAP kinase activation. Nature *383*, 547–550.

Do-Monte, F.H., Quinones-Laracuente, K., and Quirk, G.J. (2015). A temporal shift in the circuits mediating retrieval of fear memory. Nature *519*, 460–463.

Eide, B.L., Turck, C.W., and Escobedo, J.A. (1995). Identification of Tyr-397 as the primary site of tyrosine phosphorylation and pp60src association in the focal adhesion kinase, pp125FAK. Mol. Cell. Biol. *15*, 2819–2827.

Fan, L., Lu, Y., Shen, X., et al. (2018). Alpha protocadherins and Pyk2 kinase regulate cortical neuron migration and cytoskeletal dynamics via Rac1 GTPase and WAVE complex in mice. eLife *7*, 35242.

Flaherty, E., and Maniatis, T. (2020). The role of clustered protocadherins in neurodevelopment and neuropsychiatric diseases. Curr. Opin. Genet. Dev. *65*, 144–150.

Fukuda, E., Hamada, S., Hasegawa, S., et al. (2008). Down-regulation of protocadherin-α A isoforms in mice changes contextual fear conditioning and spatial working memory. Eur. J. Neurosci. *28*, 1362–1376.

Garrett, A.M., Schreiner, D., Lobas, M.A., et al. (2012). γ-protocadherins control cortical dendrite arborization by regulating the activity of a FAK/PKC/MARCKS signaling pathway. Neuron *74*, 269–276.

Giralt, A., Brito, V., Chevy, Q., et al. (2017). Pyk2 modulates hippocampal excitatory synapses and contributes to cognitive deficits in a Huntington's disease model. Nat. Commun. *8*, 15592.

Girault, J.A., Costa, A., Derkinderen, P., et al. (1999). FAK and PYK2/CAKβ in the nervous system: a link between neuronal activity, plasticity and survival? Trends Neurosci. *22*, 257–263.

Grutzendler, J., Kasthuri, N., and Gan, W.B. (2002). Long-term dendritic spine stability in the adult cortex. Nature *420*, 812–816.

Guo, Y., Xu, Q., Canzio, D., et al. (2015). CRISPR inversion of CTCF sites alters genome topology and enhancer/promoter function. Cell *162*, 900–910.

Han, S., Mistry, A., Chang, J.S., et al. (2009). Structural characterization of proline-rich tyrosine kinase 2 (PYK2) reveals a unique (DFG-out) conformation and enables inhibitor design. J. Biol. Chem. *284*, 13193–13201.

Heidinger, V., Manzerra, P., Wang, X.Q., et al. (2002). Metabotropic glutamate receptor 1-induced upregulation of NMDA receptor current: mediation through the Pyk2/Src-family kinase pathway in cortical neurons. J. Neurosci. *22*, 5452–5461.

Henley, J.M., and Nishimune, A. (2001). CAKβ/Pyk2 activates Src: another piece in the puzzle of LTP induction. Neuron *29*, 312–314.

Herry, C., and Johansen, J.P. (2014). Encoding of fear learning and memory in distributed neuronal circuits. Nat. Neurosci. *17*, 1644–1654.

Hsin, H., Kim, M.J., Wang, C.F., et al. (2010). Proline-rich tyrosine kinase 2 regulates hippocampal long-term depression. J. Neurosci. *30*, 11983–11993.

Huang, Y., Lu, W., Ali, D.W., et al. (2001). CAKβ/Pyk2 kinase is a signaling link for induction of long-term potentiation in CA1 hippocampus. Neuron *29*, 485–496.

Janak, P.H., and Tye, K.M. (2015). From circuits to behaviour in the amygdala. Nature *517*, 284–292.

Jia, Z., Li, J., Ge, X., et al. (2020). Tandem CTCF sites function as insulators to balance spatial chromatin contacts and topological enhancer-promoter selection. Genome Biol. *21*, 75.

Jia, Z., and Wu, Q. (2020). Clustered protocadherins emerge as novel susceptibility loci for mental disorders. Front. Neurosci. *14*, 587819.

Jiang, Y., Loh, Y.E., Rajarajan, P., et al. (2017). The methyltransferase SETDB1 regulates a large neuron-specific topological chromatin domain. Nat. Genet. *49*, 1239–1250.

Kinoshita, Y., Hunter, R.G., Gray, J.D., et al. (2014). Role for NUP62 depletion and PYK2 redistribution in dendritic retraction resulting from chronic stress. Proc. Natl Acad. Sci. USA *111*, 16130–16135.

Lakkakorpi, P.T., Bett, A.J., Lipfert, L., et al. (2003). PYK2 autophosphorylation, but not kinase activity, is necessary for adhesion-induced association with c-Src, osteoclast spreading, and bone resorption. J. Biol. Chem. *278*, 11502–11512.

Lambert, J.C., Ibrahim-Verbaas, C.A., Harold, D., et al. (2013). Meta-analysis of 74,046 individuals identifies 11 new susceptibility loci for Alzheimer's disease. Nat. Genet. *45*, 1452–1458.

Lee, S., Salazar, S.V., Cox, T.O., et al. (2019). Pyk2 signaling through Graf1 and RhoA GTPase is required for amyloid-β oligomer-triggered synapse loss. J. Neurosci. *39*, 1910–1929.

Lefebvre, J.L., Kostadinov, D., Chen, W.V., et al. (2012). Protocadherins mediate dendritic self-avoidance in the mammalian nervous system. Nature *488*, 517–521.

Lev, S., Moreno, H., Martinez, R., et al. (1995). Protein tyrosine kinase PYK2 involved in Ca^{2+}-induced regulation of ion channel and MAP kinase functions. Nature *376*, 737–745.

Li, J., Shou, J., Guo, Y., et al. (2015). Efficient inversions and duplications of mammalian regulatory DNA elements and gene clusters by CRISPR/Cas9. J. Mol. Cell Biol. *7*, 284–298.

Lietha, D., Cai, X., Ceccarelli, D.F., et al. (2007). Structural basis for the autoinhibition of focal adhesion kinase. Cell *129*, 1177–1187.

Loving, H.S., and Underbakke, E.S. (2019). Conformational dynamics of FERM-mediated autoinhibition in Pyk2 tyrosine kinase. Biochemistry *58*, 3767–3776.

Makuch, L., Volk, L., Anggono, V., et al. (2011). Regulation of AMPA receptor function by the human memory-associated gene KIBRA. Neuron *71*, 1022–1029.

Menegon, A., Burgaya, F., Baudot, P., et al. (1999). FAK^{+} and PYK2/CAKβ, two related tyrosine kinases highly expressed in the central nervous system: similarities and differences in the expression pattern. Eur. J. Neurosci. *11*, 3777–3788.

Montalban, E., Al-Massadi, O., Sancho-Balsells, A., et al. (2019). Pyk2 in the amygdala modulates chronic stress sequelae via PSD-95-related micro-structural changes. Transl. Psychiatry *9*, 3.

Morris, R. (1984). Developments of a water-maze procedure for studying spatial learning in the rat. J. Neurosci. Methods *11*, 47–60.

Mountoufaris, G., Canzio, D., Nwakeze, C.L., et al. (2018). Writing, reading, and translating the clustered protocadherin cell surface recognition code for neural circuit assembly. Annu. Rev. Cell Dev. Biol. *34*, 471–493.

Okigaki, M., Davis, C., Falasca, M., et al. (2003). Pyk2 regulates multiple signaling events crucial for macrophage morphology and migration. Proc. Natl Acad. Sci. USA *100*, 10740–10745.

Park, S.Y., Avraham, H.K., and Avraham, S. (2004). RAFTK/Pyk2 activation is mediated by trans-acting autophosphorylation in a Src-independent manner. J. Biol. Chem. *279*, 33315–33322.

Paul, S., Olausson, P., Venkitaramani, D.V., et al. (2007). The striatal-enriched protein tyrosine phosphatase gates long-term potentiation and fear memory in the lateral amygdala. Biol. Psychiatry *61*, 1049–1061.

Phillips, R.G., and LeDoux, J.E. (1992). Differential contribution of amygdala and hippocampus to cued and contextual fear conditioning. Behav. Neurosci. *106*, 274–285.

Ramamoorthi, K., Fropf, R., Belfort, G.M., et al. (2011). Npas4 regulates a transcriptional program in CA3 required for contextual memory formation. Science *334*, 1669–1675.

Roy, D.S., Kitamura, T., Okuyama, T., et al. (2017). Distinct neural circuits for the formation and retrieval of episodic memories. Cell *170*, 1000–1012.

Salazar, S.V., Cox, T.O., Lee, S., et al. (2019). Alzheimer's disease risk factor Pyk2 mediates amyloid-β-induced synaptic dysfunction and loss. J. Neurosci. *39*, 758–772.

Sasaki, H., Nagura, K., Ishino, M., et al. (1995). Cloning and characterization of cell adhesion kinase β, a novel protein-tyrosine kinase of the focal adhesion kinase subfamily. J. Biol. Chem. *270*, 21206–21219.

Schreiner, D., and Weiner, J.A. (2010). Combinatorial homophilic interaction between γ-protocadherin multimers greatly expands the molecular diversity of cell adhesion. Proc. Natl Acad. Sci. USA *107*, 14893–14898.

Shang, C., Liu, Z., Chen, Z., et al. (2015). A parvalbumin-positive excitatory visual pathway to trigger fear responses in mice. Science *348*, 1472–1477.

Sheehan, T.P., Neve, R.L., Duman, R.S., et al. (2003). Antidepressant effect of the calcium-activated tyrosine kinase Pyk2 in the lateral septum. Biol. Psychiatry *54*, 540–551.

Shepherd, J.D., and Bear, M.F. (2011). New views of Arc, a master regulator of synaptic plasticity. Nat. Neurosci. *14*, 279–284.

Suo, L., Lu, H., Ying, G., et al. (2012). Protocadherin clusters and cell adhesion kinase regulate dendrite complexity through Rho GTPase. J. Mol. Cell Biol. *4*, 362–376.

Thu, C.A., Chen, W.V., Rubinstein, R., et al. (2014). Single-cell identity generated by combinatorial homophilic interactions between α, β, and γ protocadherins. Cell *158*, 1045–1059.

Tonegawa, S., Liu, X., Ramirez, S., et al. (2015). Memory engram cells have come of age. Neuron *87*, 918–931.

Volk, L.J., Bachman, J.L., Johnson, R., et al. (2013). PKM-ζ is not required for hippocampal synaptic plasticity, learning and memory. Nature *493*, 420–423.

Vorhees, C.V., and Williams, M.T. (2006). Morris water maze: procedures for assessing spatial and related forms of learning and memory. Nat. Protoc. *1*, 848–858.

Wahlsten, D. (2011). Mouse Behavioral Testing: How to Use Mice in Behavioral Neuroscience (1st edn). Oxford, UK: Academic Press, Elsevier.

Wu, C.T., Haggerty, D., Kemere, C., et al. (2017). Hippocampal awake replay in fear memory retrieval. Nat. Neurosci. *20*, 571–580.

Wu, Q., and Jia, Z. (2021). Wiring the brain by clustered protocadherin neural codes. Neurosci. Bull. *37*, 117–131.

Wu, Q., and Maniatis, T. (1999). A striking organization of a large family of human neural cadherin-like cell adhesion genes. Cell *97*, 779–790.

Xu, C., Krabbe, S., Grundemann, J., et al. (2016). Distinct hippocampal pathways mediate dissociable roles of context in memory retrieval. Cell *167*, 961–972.

Yu, H., Li, X., Marchetto, G.S., et al. (1996). Activation of a novel calcium-dependent protein-tyrosine kinase. Correlation with c-Jun N-terminal kinase but not mitogen-activated protein kinase activation. J. Biol. Chem. *271*, 29993–29998.

Zagrebelsky, M., Holz, A., Dechant, G., et al. (2005). The p75 neurotrophin receptor negatively modulates dendrite complexity and spine density in hippocampal neurons. J. Neurosci. *25*, 9989–9999.